IOP Publishing Flex. Print. Electron. 9 (2024) 025002 https://doi.org/10.1088/2058-8585/ad2db0

Flexible and Printed Electronics

PAPER

Applicability of normalized resistance rate model for predicting fatigue life and resistance evolution in composite conductive inks

Qiushi Li, Olivier Pierron* and Antonia Antoniou*

G.W. Woodruff School of Mechanical Engineering, Georgia Institute of Technology, Atlanta, GA 30318, United States of America
* Authors to whom any correspondence should be addressed.

E-mail: olivier.pierron@me.gatech.edu and antonia.antoniou@me.gatech.edu

Keywords: model, composite conductor, fatigue, cyclic loading, design

OPEN ACCESS

RECEIVED
21 October 2023

REVISED
1 February 2024

ACCEPTED FOR PUBLICATION
27 February 2024

PUBLISHED
11 April 2024

Abstract

The electrical resistance of metal-polymer conductive inks increases as they undergo cyclic loading, posing a major challenge to their reliability as interconnect materials for flexible electronic devices. To characterize an ink's fatigue performance, extensive electro-mechanical testing is usually performed. Phenomenological models that can accurately predict the resistance increase with cyclic loading can save time and be useful in flexible conductor design against fatigue failure. One such model was recently developed for only one composite ink type. The model is based on experiments monitoring resistance under monotonic stretch data and multiple experiments measuring the rate of increase of the resistance under different strain amplitudes and mean strains. The current work examines whether such resistance rate model could be generalized to apply for more types of composite inks. Two composite inks with different binder material, metal flake sizes and shapes, and substrate material were experimentally tested under monotonic and cyclic loading. It was found that the two new inks are also more sensitive to strain amplitude than mean strain. The resistance rate model accurately predicts early/catastrophic failure (<1000 cycles) in all inks and conservatively estimates high fatigue life for low strain amplitudes. A protocol detailing the procedures for applying the resistance model to new inks is outlined.

1. Introduction

Flexible hybrid electronics devices represent a unique category of electronics known for their ability to conform to body surfaces, primarily finding applications in wearable healthcare devices [1–4]. These devices utilize compliant circuitry with conductive interconnects to transmit electrical signals while adapting to and deforming with non-conformal surfaces. In typical wearable devices, they are subjected to repeated stretching of up to 30% tensile strain [5]. A significant challenge in designing interconnect materials lies in maintaining electrical conductivity after enduring repeated loading within the expected strain range for the application.

Several conductive interconnect materials have been studied for their electrical performance under repeated deformation, including thin metal films [6–11], metal nanoparticle inks [12–15], graphene composites [16] and metal-polymer composite inks [17–23]. Compliant circuitry is commonly created by depositing a thin interconnect material layer on a thicker substrate. One example of such an interconnect material is the metal-polymer conductive ink, which incorporates micron-sized metal flakes within a compliant polymer binder. This composite conductive ink is subsequently applied to a compliant polymer substrate, typically through screen printing.

Unlike metal thin films, composite metal-polymer inks do not experience sudden rupture [24–32] or fatigue failure [9, 10, 33] at low tensile strain levels (<10%) while deposited on compliant (polymer) substrates. Therefore, composite inks are able to maintain electrical conductivity at higher applied strains provided they are deposited on an adequately stiff polymer substrate [23, 34, 35]. The fatigue behavior of composite conductive inks is less well studied, with the exception of Dupont's PE874 [17, 23] where cracks were found to form and continually

Table 1. Table of symbols.

Symbols	Description
ε	Tensile strain
ε_m	Mean strain for cyclic test
ε_a	Strain amplitude for cyclic test
R	Measured resistance during testing (adjusted for clamped portion of specimen)
R_0	Measured resistance prior to testing (adjusted for clamped portion of specimen)
$(R/R_0)_{fail}$	Failure threshold R/R_0 for a monotonic test.
ε_f	Monotonic tensile strain at which $(R/R_0)_{fail}$ is reached
R_{max}	Maximum measured R during a cycle
N	Number of cycles in a fatigue test
$(R/R_0)'$	Normalized resistance rate change in R_{max}/R_0 with cycling, or $d(R_{max}/R_0)/dN$
$(R/R_0)'_{char}$	Characteristic normalized resistance rate $(R/R_0)'$ for a cyclic test
$(R/R_0)'_{min}$	Minimum normalized resistance rate $(R/R_0)'$ over the cycles for a cyclic test
$(R_{max}/R_0)_{N=1}$	R_{max}/R_0 for the first cycle
$(R_{max}/R_0)_{fail}$	Failure threshold R_{max}/R_0 for a cyclic test
$(R_{max}/R_0)_{modeled}$	Modeled R_{max}/R_0 at cycle N for a cyclic test
$(N_f)_{modeled}$	Modeled fatigue life as defined the number of cycles until $(R_{max}/R_0)_{fail}$ is reached according to model
$R_{full\ specimen,\ \varepsilon}$	Measured resistance at tensile strain ε without adjustment for clamped portion of specimen
$R_{full\ specimen,\ \varepsilon=0}$	Measured resistance at zero tensile strain without adjustment for clamped portion of specimen
d_{grips}	Distance between grips
l_{print}	Effective length of double trace lines

deepen during cyclic loading. For that ink, Li *et al* [36] recently proposed a resistance rate model for predicting PE874's fatigue behavior. It is unclear whether that model/approach could be used for other composite inks with different metal flakes, binder or substrate materials. For this to be explored, the electrical resistance of other inks needs to be experimentally obtained during monotonic and cyclic loading following Li's [36] process, as described below. Table 1, provides a list of symbols used in this manuscript.

The electrical degradation of a conductive ink trace during an electro-mechanical test can be characterized by the normalized resistance R/R_0, which is the resistance R measured during testing normalized with respect to the initial resistance R_0 of the ink trace measured prior to the experiment. In monotonic stretch experiments, the normalized resistance is plotted as a function of the applied strain. Multiple experiments under different combinations of mean strain, ε_m, and strain amplitude, ε_a, are needed for the model calibration. Typically, the experiments are performed between a maximum, $\varepsilon_{max} = \varepsilon_m + \varepsilon_a$, and minimum $\varepsilon_{min} = \varepsilon_m - \varepsilon_a$ strain range. During a cyclic stretch test, the maximum R/R_0 during each cycle, or R_{max}/R_0, occurs at the maximum strain value, ε_{max}. The rate of change in R_{max}/R_0 with cycling, or $d(R_{max}/R_0)/dN$ (where N is the number of cycles), was found by Li *et al* [36] to be a particularly relevant parameter for characterizing R/R_0 increase with cycling. The rate $d(R_{max}/R_0)/dN$ will be referred to as $(R/R_0)'$ for shorthand.

A constant rate model was proposed by Li *et al* [36] to predict the evolution of R_{max}/R_0 for N cycles. The model takes input parameters from several monotonic and cyclic stretch tests to create a prediction of $R_{max/}R_0$-cycles evolution for a cyclic test with any given ε_m and ε_a within the modeled range, as shown by the schematic in figure 1. The monotonic stretch tests are used to obtain an average polynomial fit for R/R_0 evolution with applied tensile strain ε (figure 1), which is then used to model R_{max}/R_0 at the tensile strain $\varepsilon_m + \varepsilon_a$ during the first cycle of the cyclic test. For subsequent cycles, a constant characteristic $(R/R_0)'_{char}$ is assumed for cyclic tests at a given ε_a. From several cyclic tests performed at different ε_a, a power law function can be fitted for the relation between $(R/R_0)'_{char}$ and ε_a (figure 1). The fit for $(R/R_0)'_{char}$ as a function of ε_a can be used to obtain $(R/R_0)'_{char}$ for any ε_a within the modeled range. The modeled range of strains (and therefore the range of strains to be used for the input cyclic tests) can be roughly determined by considering R/R_0-ε evolution from the monotonic tests and the failure tensile strain ε_f at which the failure criterion $(R/R_0)_{fail}$ is reached (figure 1). The modeled R_{max}/R_0 for N cycles is given as follows.

$$\left(\frac{R_{max}}{R_0}\right)_{modeled} = \left(\frac{R_{max}}{R_0}\right)_{N=1} + (N-1)\left(\frac{R}{R0}\right)'_{char}. \quad (1)$$

The model can also be used to predict fatigue life as defined by the number of cycles until a failure threshold for R_{max}/R_0 is reached according to the model. If failure is defined by $(R_{max}/R_0)_{fail}$, then the predicted fatigue life $(N_f)_{modeled}$ is:

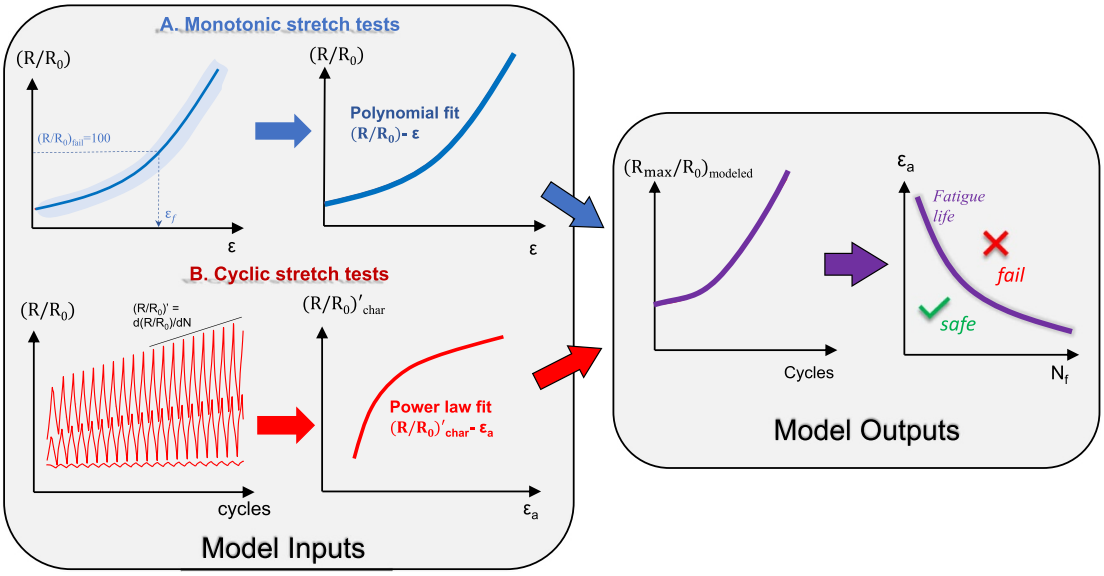

Figure 1. Schematic of model inputs and outputs. Inputs are the average polynomial fit for R/R_0-ε from monotonic stretch tests and power law fit for $(R/R_0)'$-ε_a from cyclic stretch tests; outputs are the predicted R_{max}/R_0-cycles evolution and ε_a-N_f, as described in the work of Li *et al* [36].

$$(N_f)_{modeled} = \frac{\left(\frac{R_{max}}{R_0}\right)_{fail} - \left(\frac{R_{max}}{R_0}\right)_{N=1}}{\left(\frac{R}{R_0}\right)'_{char}} + 1. \quad (2)$$

Depending on what the designer determines as the critical $(R_{max}/R_0)_{fail}$ then multiple fatigue life curves can be generated and can be used to design inks against fatigue failure. The safe parameter space is defined as strain amplitudes that are well below the fatigue life curve, as seen in the schematic of figure 1.

The rate model proposed by Li *et al* [36] offers reasonable predictions of resistance evolution with cyclic stretching for a wide range of ε_m and ε_a, based on only 5–6 cyclic stretch tests and several monotonic tests. The model has the potential to greatly reduce the amount of experiment time needed to characterize R/R_0-cycles evolution in a conductive ink, especially considering that only tens of cycles may be needed to be obtain the characteristic $(R/R_0)'$ parameter for a cyclic test. However, the model was only shown to be applicable for one ink type. The current work explores the applicability of the model for two other silver-based composite inks with different binder materials and different flake sizes and shapes than that reported in [36]. Specifically, this work describes an experimental investigation of monotonic and cyclic behavior of flexible conductive inks and demonstrates that the rate model described by Li *et al* [36] can be applicable to wider categories of flexible inks.

2. Experiment and modeling methods

2.1. Fabrication of test materials

Figure 2(a) shows the two new inks examined in this work are Dupont's 5025 and a developmental conductive ink (N-ink1). The experimental results are compared along with the PE874 ink results from the work of Li *et al* [23, 36] (ink also shown on figure 2(a)). Both the PE874 and 5025 inks are deposited on their respective substrate layers by a screen-printing process performed at the DuPont Applications Laboratory using optimized printing processes. Details of the screen-printing processes for the inks can be found in the previous works by Cahn *et al* [34] and Li *et al* [36]. In the current work, the 5025 ink had a single ink layer printed in one printing pass with a thickness of about 10 μm; the PE874 ink had two ink layers printed in two separate printing passes with a total thickness of about 20 μm. There was no visible separation between the two PE874 ink layers based on SEM (scanning electron microscope) images of the focused ion beam (FIB) cross-section, nor was there delamination between the two ink layers during previous in-situ SEM mechanical tests [23]. The PE874 and 5025 inks used the same type of Ag flakes, which were sized from 100 s of nm to several μm (figures 3(a), (b) and (d), (e)). The PE874 ink used a polyurethane binder material, while the 5025 ink used an acrylic binder material. The fraction of total ink volume occupied by the Ag inks is slightly higher for the PE874 ink at 55%, compared to 49% for the 5025 ink [34]. There is also a significant volume of μm-sized voids in PE874 ink with a total void volume fraction of 17% [34], while the 5025 ink does not have any noticeable voids. From the FIB cross-section images of N-ink1 (figures 3(c)–(f)), it can be observed that the ink consists of larger-sized type of Ag flakes. The average Ag flake size is ~2 μm, the solid flake fraction is found to be ~70%. There is also a substantial number of voids in the binder (>10%). The ink binder is compliant with stiffness similar to thermoplastic polyurethane (TPU). The

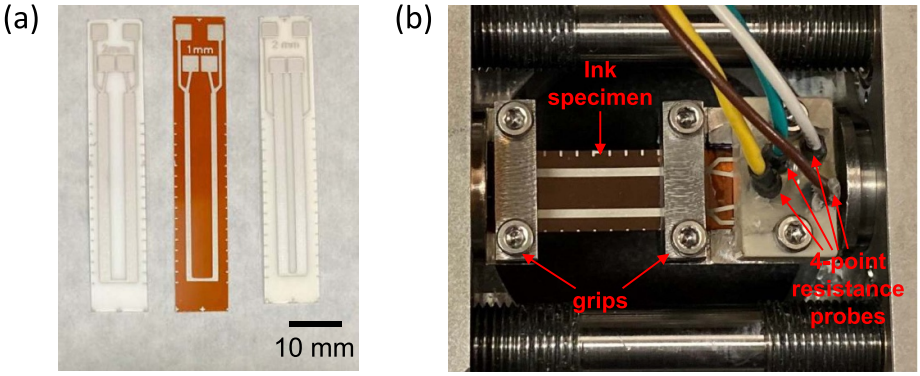

Figure 2. (a) Optical images of the PE874-TPU, 5025-PI, and Nink1-TPU specimens from left to right; (b) testing frame used for monotonic and cyclic stretch testing. The ink specimen is stretched between the two grips, while synchronous resistance measurements are made using the 4-point resistance probes. Trace width is 2mm in 2(b).

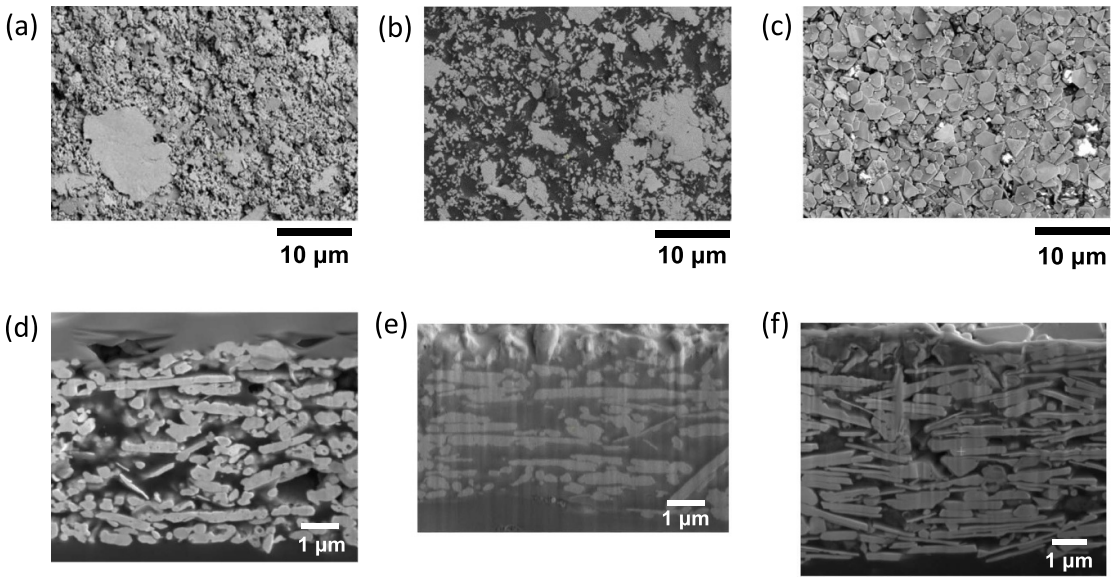

Figure 3. Top view SEM images of (a) PE874 ink, (b) 5025 ink, and (c) Nink-1; FIB cut cross-section view images of (d) PE874 ink, (e) 5025 ink, and (f) Nink-1. Note that all 3 inks have silver flakes with different binder materials.

Table 2. Details of the experiments performed for the 3 different inks. The experimental results with PE874 ink were from the work by Li *et al* [23, 36].

	PE874	5025	Nink1
Trace line width (mm)	2 mm	1 mm	2 mm
Ink thickness	2-layer (∼20 μm)	1-layer (∼10 μm)	1-layer (∼20 μm)
Substrate material	TPU (TE-11C)	PI (Kapton)	TPU
Substrate thickness	∼90 μm	∼130 μm	∼100 μm
Cyclic tests ($\varepsilon_m \pm \varepsilon_a$)	15 ± 1%, 15 ± 2%, 60 ± 2%, 15 ± 5%, 10 ± 10%, 30 ± 12%, 30 ± 15%, 65 ± 15%, 30 ± 18%	15 ± 1%, 5 ± 2%, 15 ± 2%, 15 ± 5%, 15 ± 8%	15 ± 1%, 5 ± 2%, 15 ± 2%, 15 ± 5%, 15 ± 8%, 15 ± 10%

thickness of the Nink1 layer is about 20 μm. The PE874 ink was printed onto the TE-11C TPU substrate which has a thickness of about 90 μm, while the Nink-1 was printed onto a different TPU substrate which has a thickness of 100 μm. The 5025 ink was printed onto a Kapton polyimide (PI) substrate which has a thickness of about 130 μm. Table 2 summarizes the specimen geometries and cyclic tests performed for each ink. The stretch test ink specimens were printed in U-shaped, double trace lines with 2 mm trace width for the PE874 ink and N-ink1, and 1 mm trace width for the 5025 ink (figure 2(a)). The four pads

in the print pattern were designed for the four-point electrical resistance probes.

2.2. Monotonic and cyclic stretch testing procedures

The monotonic and cyclic uniaxial stretch tests were performed with synchronous electrical resistance measurements on the Linkam Scientific TST350 Microtensile test stage at a strain rate of 2% per second for the PE874 ink and N-ink1 specimens, and on the Kammrath & Weiss MZ0-1 tensile test stage at a strain rate of 0.133% per second for the 5025 ink specimens. The 5025 ink specimens were tested on the Kammrath & Weiss test stage due to the high stiffness of the PI substrate requiring a higher load capacity. For 5025 on PI, due to the high substrate stiffness, the experiments were stopped close to the load limit of the load cell. For that ink this corresponded to ~70% applied strain. For both tensile stages, the electrical resistance is measured synchronously during the stretch tests using the Agilent 34401 A digital multimeter. Figure 2(b) shows a close-up view of the testing setup with the pads for the simultaneous measurement of resistance, as the sample is secured between the grips and tested. The cyclic stretching tests were performed by first stretching the test specimen to the maximum strain $\varepsilon_m + \varepsilon_a$, and then cycling between the maximum strain $\varepsilon_m + \varepsilon_a$ and minimum strain $\varepsilon_m - \varepsilon_a$.

For the PE874 and 5025 ink specimens, the distance d_{grips} between the specimen grips (about 30 mm) is shorter than half the effective length l_{print} of the double trace lines (38 mm). The Nink-1 specimens were redesigned so that $l_{print}/2$ is about the same as d_{grips}. For both specimen designs, the initial resistance R_0 was adjusted to account for the difference between $l_{print}/2$ and d_{clamp}.

$$R_0 = R_{\text{full specimen, }\varepsilon=0} \times \left(\frac{d_{grips}}{l_{print}/2}\right). \quad (3)$$

The resistance R is the sum of the initial resistance R_0 and the measured change in resistance ΔR, which is entirely attributed to the strained portion of the specimen

$$\Delta R = R_{\text{full specimen},\varepsilon} - R_{\text{full specimen},\varepsilon=0} \quad (4)$$

$$R = R_0 + \Delta R. \quad (5)$$

3. Results and discussion

3.1. Determination of normalized resistance-strain evolution

Figure 4 shows the R/R_0 evolution with applied strain for the three different inks from several monotonic stretch tests. The solid lines represent the average 4th order polynomial fits for the curves with the shaded regions marking the standard deviation of the different monotonic experiments. The average polynomial fit for each ink is obtained by averaging the polynomial fits from individual monotonic stretch tests. According to the schematic of figure 1, the average polynomial fit is used to estimate R/R_0 at the maximum strain $\varepsilon_m + \varepsilon_a$ during the first cycle. The R/R_0-strain data for each ink can also be used to estimate the usable range of tensile strains according to an R/R_0 failure criterion. In our prior work [36], $R/R_0 = 100$ was chosen as the failure criterion for the PE874 ink. For consistency, we employ the same failure criterion $(R/R_0)_{fail} = 100$. The criterion is used to establish the usable range of strains for the inks from the monotonic curves of figure 4. It is found that the useable range for Nink-1 specimen, e.g. before the $R/R_0 < (R/R_0)_{fail}$, is smaller than that of the PE874 and 5025 inks. For N-ink1, R/R_0 increases much more rapidly with applied strain, reaching a R/R_0 of 100 at about 40% strain, whereas PE874 reaches $(R/R_0)_{fail}$ closer to 100% applied strain. It should be noted that the R/R_0 increase with monotonic or cyclic stretching does not depend solely on the ink material, but also on the ink and substrate geometry (width and thickness) as well as the substrate material. Therefore, the quantitative modeling of R/R_0 increase with cyclic stretching will be affected by these factors.

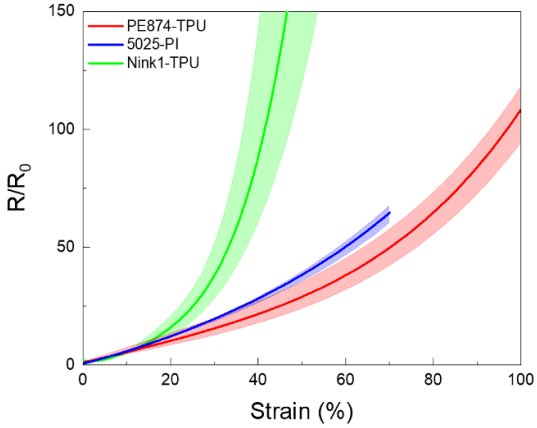

Figure 4. Measured R/R_0-ε evolution from monotonic stretch tests, for all 3 inks. The light-colored regions mark the range of variation in measured R/R_0 data from multiple tests; the colored lines are the average polynomial fits.

3.2. Determination of $(R/R0)'_{char}$ from R/R0-cycles evolution

Figure 5 shows the normalized resistance R/R_0 change for multiple cycles (N) for the same mean strain but different strain amplitudes for the three different inks. Figure 5(a) shows the results from the cyclic tests with $\varepsilon_m \pm \varepsilon_a = 15 \pm 1\%$. Figure 5(b) shows the results for cyclic tests with $\varepsilon_m \pm \varepsilon_a = 15 \pm 5\%$ for all 3 inks. The cyclic tests performed at $\varepsilon_a = 1\%$ are representative

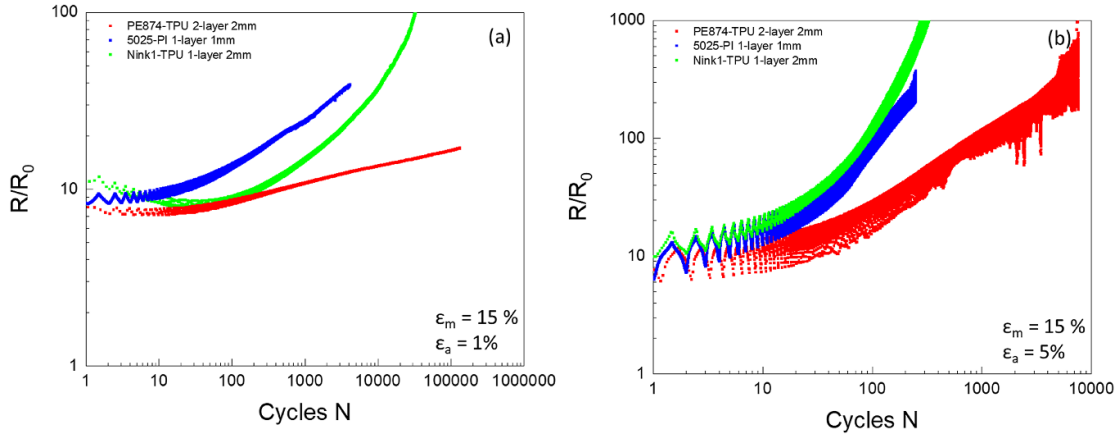

Figure 5. Measured evolution of normalized resistance R/R_0 as a function of cycles for a mean strain, $\varepsilon_m = 15\%$ but different strain amplitude, ε_a. In the left panel (a) $\varepsilon_a = 1\%$, and the right panel (b) $\varepsilon_a = 5\%$, for the different inks.

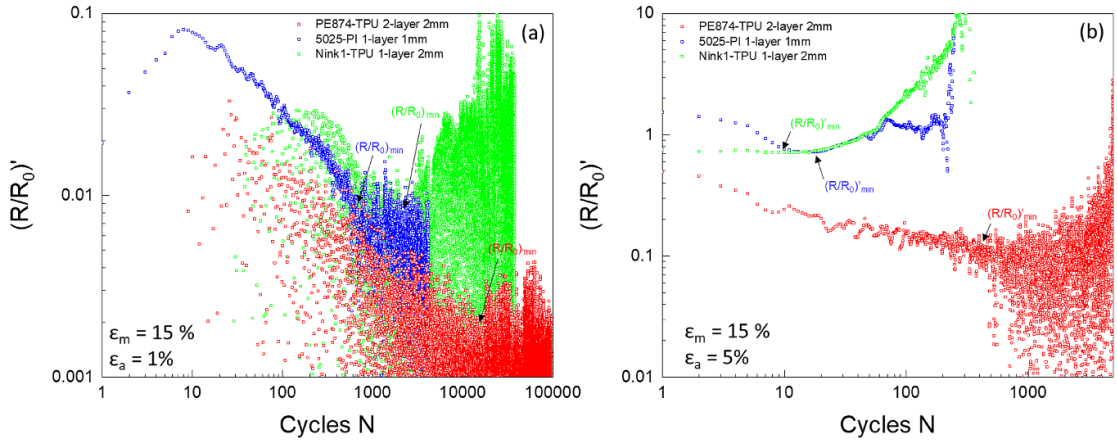

Figure 6. The rate of change of the normalized resistance $(R/R_0)'$ as a function of cycles for a mean strain, $\varepsilon_m = 15\%$ but different strain amplitude, ε_a. In the left panel (a) $\varepsilon_a = 1\%$,and the right panel (b) $\varepsilon_a = 5\%$, for the different inks.

of the normalized resistance evolution at low strain amplitudes ($\varepsilon_a \leqslant 2\%$,) while the tests performed at $\varepsilon_a = 5\%$ are representative of the normalized resistance evolution at medium to high strain amplitudes. R/R_0 generally increases steadily over the cycles until instability in R/R_0 is reached. Instability is defined as rapid normalized resistance growth. It can be readily seen that R/R_0 increases much more quickly (by several orders of magnitude) when the strain amplitude is higher. For the $\varepsilon_a = 1\%$ tests with the PE874 ink and Nink-1, the normalized resistance, R/R_0 decreased in the first few cycles. This is possibly due to the relaxation of the TPU substrate while the fatigue damage was not large significant to counteract the relaxation.

The rate of change in R/R_0 with cycling, or $(R/R_0)'$, quantifies the normalized resistance growth rate with cycling and is a key parameter for the predictive model developed by Li *et al* [36]. In our work we follow the same process so that $(R/R_0)'$ at cycle N is determined by a linear regression fit of the maximum R/R_0 per cycle-to-cycles data from cycles N-4 to N + 4, excluding any null points at the beginning or end of the set. The choice of using cycles N-4 to $N + 4$ for the linear regression fit was made by trial to achieve a generally smooth $(R/R_0)'$ evolution over the cycles. Using this definition of $(R/R_0)'$, the evolution of $(R/R_0)'$ over cycles was obtained from the R/R_0-cycles data. For any cycle, the data point of greatest interest is the maximum R/R_0 during the cycle, or R_{max}/R_0. For the rest of the discussion, $(R/R_0)'$ will refer to the rate of change in R_{max}/R_0, or $(R_{max}/R_0)'$. Figure 6 shows the rate of normalized resistance $(R/R_0)'$ change with cycling by obtaining the slope of the R/R_0-cycles data shown in figure 5. For the $\varepsilon_a = 1\%$ tests, $(R/R_0)'$ is very low or negative in the first few cycles, and then increases to a local maximum during the first 100 cycles. For the $\varepsilon_a = 1\%$ tests with the PE874 and 5025 inks, a steady state minimum $(R/R_0)'$was

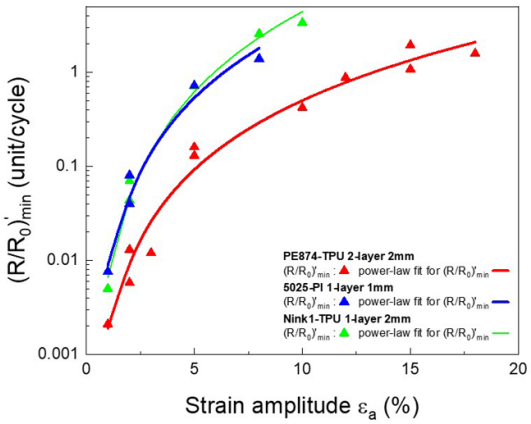

Figure 7. The minimum normalized resistance rate $(R/R0)'_{min}$ for different ε_a for the two new inks compared against Li *et al* [23, 36] dataset. The power law fits for all 3 inks are shown as solid lines.

eventually reached, at least within the tested cycle range. For the $\varepsilon_a = 1\%$ tests with Nink-1, $(R/R_0)'$ increased again after reaching the minimum at about cycle 2000. For the $\varepsilon_a = 5\%$ tests, $(R/R_0)'$ is at a local maximum at cycle 1 and then steadily decreases until a minimum $(R/R_0)'$ is reached, after which $(R/R_0)'$ increases again until instability is reached. This trend in the evolution of $(R/R_0)'$ with cycles is consistent for all the 3 tested inks at medium and high strain amplitudes.

The Li *et al* model assumes that $(R/R_0)'$ is constant over all cycles until failure since it was determined that a rapid increase in the rate of normalized resistance occurs near the instability point. Hence a characteristic $(R/R_0)'$ needs to be defined for a fatigue test at given ε_m and ε_a values. In the current work, the characteristic $(R/R_0)'$ is defined as the minimum rate $(R/R_0)'$, or $(R/R_0)'_{min}$, over the cycles. For both the high and low strain amplitude tests shown in figure 6, there exists a minimum $(R/R_0)'$ over the cycles, which in many cases represented a steady state $(R/R_0)'$. In figure 6, $(R/R_0)'_{min}$ is labeled for each of the shown tests. For the $\varepsilon = 1\%$ tests, there is significant local fluctuation in the $(R/R_0)'$ data due to the low rates involved. For such low strain amplitude cases, the $(R/R_0)'_{min}$ over the cycles is defined along the top edge of the $(R/R_0)'$ vs. cycles envelop. Figure 7 shows that single minimum normalized resistance rate $(R/R_0)'_{min}$ measurement for more cyclic experiments than those presented in figure 6. For each ink, there exists a strong correlation between $(R/R_0)'_{min}$ and strain amplitude, ε_a. A power-law function fit is also shown as a solid line for each ink type. The fit function between $(R/R_0)'_{min}$ and ε_a assumes that $(R/R_0)'_{min}$ depends only on ε_a rather than both ε_a and ε_m. The $(R/R_0)'_{min}$ data from the cyclic tests with all 3 inks show that this is generally a valid assumption. For all 3 inks, separate fatigue tests were performed at different ε_m with the same strain amplitude of $\varepsilon_a = 2\%$ but different ε_m, which were 15% and 60% for the PE874 tests and 5% and 15% for both the 5025 and Nink-1 tests. For the PE874 ink, separate tests were also performed at $\varepsilon_a = 15\%$ for different ε_a at 30% and 65%. It was found that there was at most 2–3 times difference in $(R/R_0)'_{min}$ between drastically different mean strains for all inks. As figure 7 shows, the difference in $(R/R_0)'_{min}$ for strain amplitudes in the range of 1%–20% can be more than 1000 times. Finally, the minimum normalized resistance rate curves for two inks, e.g. Nink-1 and 5025, appear to be very close to each other and have a higher sensitivity to the strain amplitude than PE 874. Indeed, the minimum normalized resistance rate at a strain amplitude of 5%, is ~10 times greater for the newly tested inks than PE 874.

3.3. Model predictions for the evolution of normalized resistance R/R_0 with cycles and fatigue life

Figures 8–10(a) show the predicted and measured R_{max}/R_0 as a function of cycles (in a semi-log format) for PE874 ink, 5025 ink, and N-ink1, respectively. For all inks, the model predictions for R_{max}/R_0 with cycles closely matched the measured data for the first 1000 cycles, where inks subjected to higher strain amplitudes tend to fail. Beyond 1000 cycles, the predicted evolution began to show more deviation from the measured data. The high cycle behavior occurs for inks tested under low strain amplitudes ε_a. The discrepancy between the measured and predicted evolutions for the low ε_a cases is most likely due to the larger spread in $(R/R_0)'$. Since $(R/R_0)'_{min}$ was defined along the upper edge of the $(R/R_0)'$ envelop, the predicted $(R/R_0)'$ vs. cycles for the low ε_a cases were expected to be conservative compared with the measured data.

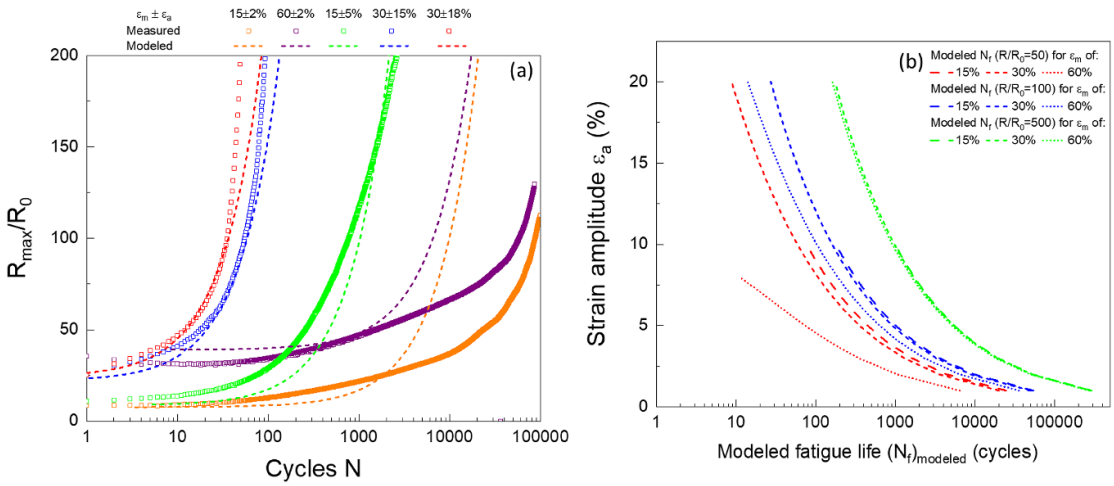

Figure 8. For the PE874 on TPU from Li *et al* [23, 36]: (a) A comparison between the experimentally measured -data points- and the modeled values -dotted lines- for the normalized resistance $(R/Ro)_{max}$ as a function of cycles for different cyclic tests. (b) For that same ink, the model predictions for the strain amplitude-life curves using three different $(R/Ro)_{fail}$ criteria and different levels of mean strain.

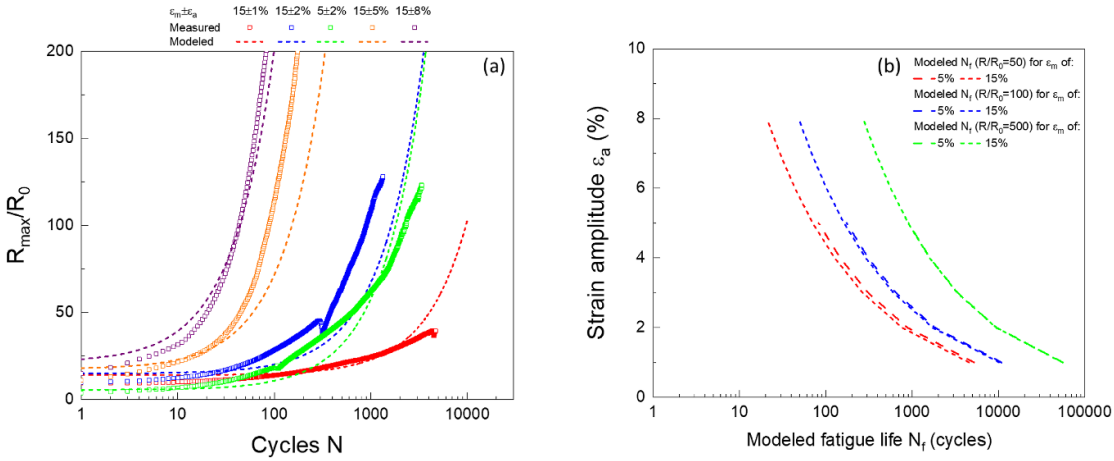

Figure 9. For the 5025 on PI: (a) A comparison between the experimentally measured -data points- and the modeled values -dotted lines- for the normalized resistance $(R/Ro)_{max}$ as a function of cycles for different cyclic tests. (b) For that same ink,the model predictions for the strain amplitude-life curves using three different (R/Ro)tai 1 criteria and different.

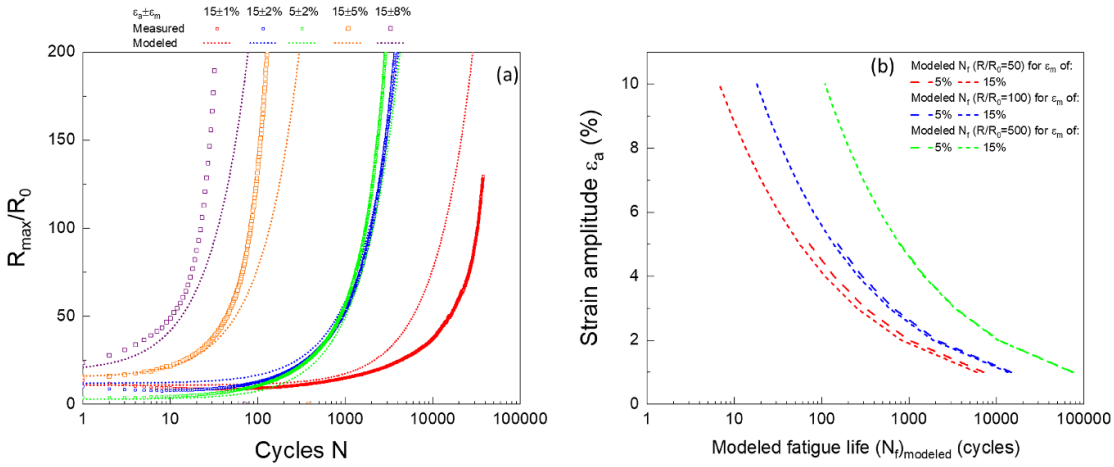

Figure 10. For Nink-1on TPU: (a) A comparison between the experimentally measured -data points- and the modeled values -dotted lines- for the normalized resistance $(R/Ro)_{max}$ as a function of cycles for different cyclic tests. (b) For that same ink,the model predictions for the strain amplitude-life curves using three different $(R/Ro)_{tail}$ criteria and different.

As discussed in the introduction and illustrated in the figure 1 schematic, the model can also be used to predict the ink fatigue life as defined by the number of cycles until the failure threshold $(R/R_0)_{fail}$. Although a $(R/R_0)_{fail}$ of $R/R_0 = 100$ was used by Li *et al* [23, 36], other $(R/R_0)_{fail}$ could also be defined. The model can predict N_f for any $(R/R_0)_{fail}$ by modifying equation (2). For each of the 3 inks, figures 8–10(b) show the predicted fatigue life $\widehat{N}_f$ for different imposed strain amplitudes ε_m and different ε_m. The colors indicate different $(R/R_0)_{fail}$ values from 50 to 500. From the $\widehat{N}_f$ predictions for the PE874 ink in figure 8(b), it can be observed that for low failure resistance $(R/R_0)_{fail}$ ($\sim$50), the effect of ε_m on the $\widehat{N}_f$ predictions becomes significant. This is due to the fact that a low $(R/R_0)_{fail}$ is close to the first cycle normalized resistance value $(R/R_0)_{N=1}$ for a high ε_m. This is corroborated by the measured R_{max}/R_0 vs. cycles for the 60 $\pm$ 2% and 15 $\pm$ 2% tests (figure 8(a)), which showed a much larger difference in measured N_f according to $(R/R_0)_{fail} = 50$ than to $(R/R_0)_{fail} = 100$. When ε_m is low ($\leqslant$15%), the effect of ε_m on the predicted N_f is minor regardless of the $(R/R_0)_{fail}$ used. This is corroborated by the measured R_{max}/R_0-cycles evolutions for the 5 $\pm$ 2% and 15 $\pm$ 2% tests for both the 5025 ink and N-ink1. Therefore, the choice of $(R/R_0)_{fail}$ could be different depending on the level of ε_m. The model has the advantage of being able to predict fatigue life for any given $(R/R_0)_{fail}$.

The general closeness between the predicted and measured R/R_0 vs cycles curves for all 3 inks (figures 8–10(a)) show that the model is applicable to a variety of different inks and substrates across the range of strains expected for the ink applications. The tested inks differed by the Ag flake size and shape, binder material, as well as porosity in the ink microstructure. The PI substrate used with the 5025 ink was much stiffer than the TPU substrates used with the PE874 ink and Nink-1 and had significantly more plastic deformation as it is cyclically stretched. Despite these differences in the ink and substrate materials, the model provided reasonable predictions of the normalized resistance change R/R_0 with cycles *especially* for conditions where ink can fail after a small number of cycles ($<$1000).

Therefore, the model was found to accurately capture the behavior of 3 different inks, giving close predictions for their behavior under high strain amplitudes.

3.4. Model calibration/process for composite conductive inks

From a practical perspective, the model is applicable to many inks. Based on the experiments performed for the three different inks we can define a process for calibrating model parameters to obtain fatigue life predictions for many other composite inks. The calibration involves only several monotonic stretch tests and about 6 or 7 cyclic tests so that the R/R_0 evolution with cyclic stretching can be reasonably characterized for a given ink. The model also effectively incorporates the effect of ε_m even if this is a secondary effect for all 3 inks compared in this manuscript. Figure 11 shows a flowchart detailing the steps for calibrating the model parameters to obtain fatigue life predictions for composite inks. The first sequence involves performing several monotonic stretch tests, with the number of tests depending on how consistent the measured R/R_0 vs applied strain ε. The R/R_0 vs ε results from the monotonic tests serve two purposes. The first is to obtain an average polynomial fit for R/R_0 as a function of applied strain ε, which is used to model R_{max}/R_0 at the maximum strain $\varepsilon_m + \varepsilon_a$ during the first cycle of the cyclic test. The second purpose is to estimate the range of maximum strain to be considered for the cyclic stretch tests, according to the tensile strain ε_f at which the failure threshold $(R/R_0)_{fail}$ is reached during monotonic testing. After the monotonic experiments, a series of cyclic stretch tests across different ε_a need to be performed, including at least one test at a different ε_m value. After obtaining the evolution of $(R/R_0)'$ for different cyclic test conditions the following checks need to be made. The designer needs to ascertain whether (1) $(R/R_0)'_{char}$ is significantly affected by ε_m and (2) check whether the $(R/R_0)'$ values are too low ($<$1). If there is a significant mean strain effect on $(R/R_0)'_{char}$, the current model will not be sufficient in predicting R/R_0 evolution without performing more cyclic tests and obtaining the $(R/R_0)'_{char}$-ε_a fit function for multiple ε_m values. If the normalized resistance rate $(R/R_0)'$ is too low, more cyclic tests at higher ε_a may need to be performed since catastrophic failures tend to occur when the rate of growth of the normalized resistance $(R/R_0)'>1$. If the mean strain effect on $(R/R_0)'_{char}$ remains secondary and the $(R/R_0)'$ values are adequately high, a power law function can be fit between $(R/R_0)'_{char}$ and ε_a. Using the average polynomial fit from the monotonic R/R_0 vs ε and power law fit for $(R/R_0)''_{char}$-ε_a from the cyclic tests the model can be calibrated. It can then be used to predict R_{max}/R_0 evolution with cycling for any given ε_m and ε_a combination within the range of the model calibration parameters. Finally, we note that the model describes macroscopic measurements of ink properties and does not look into details of fatigue mechanisms, which could be different for each ink. This could be an excellent topic for a follow-up study.

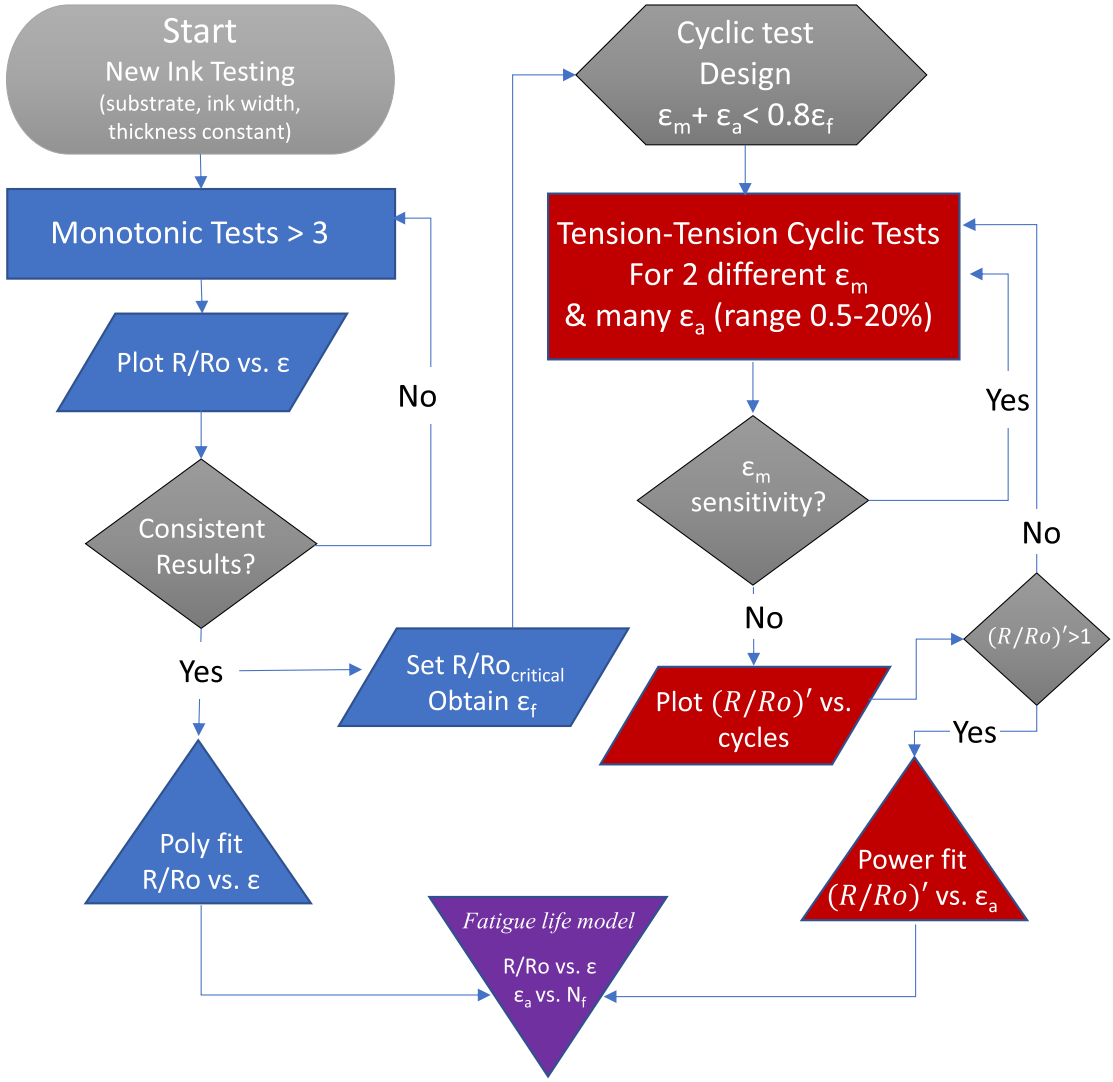

Figure 11. Flow chart for characterizing the electrical performance of a conductive ink with cyclic stretching using the model, based on information drawn from a few monotonic and cyclic stretch tests.

4. Conclusions

The applicability of a constant normalized resistance rate model developed by Li *et al* [36] was explored for two additional composite ink types: Dupont's 5025 ink, and a developmental ink, N-ink1. These new inks are fabricated using silver flakes of different shapes, amounts as well as different binder materials. In order to test the model applicability, different monotonic and cyclic stretch tests were performed and these experiments were used to obtain relevant model parameters.

1) The model is applicable to a variety of different ink and substrate materials. The tested composite inks differed in Ag flake size and shape, binder material, porosity, as well as substrate material. A general closeness between the measured and predicted R/R_0 vs. cycles was achieved for all tested inks.
2) The model can save time on the electromechanical testing needed to characterize a conductive ink. With only several monotonic stretch tests and about 6 or 7 fatigue tests, the R/R_0 vs. cycles can be obtained for a given ink.
3) The model is based on experimentally informed assumptions, and effectively captures the effect of both ε_m and ε_a on the behavior of the R/R_0 with cycling. A power law fit function between the $(R/R_0)'_{min}$ and ε_a can be used to interpolate $(R/R_0)'_{min}$ for any ε_a within the fitted range, assuming the dependence of $(R/R_0)'$ on only ε_a. The effect of ε_m is incorporated through its effect on R_{max}/R_0 during the first cycle.
4) The model is versatile in being able to predict fatigue life according to different $(R/R_0)_{fail}$ criteria. A testing protocol was developed to calibrate model parameters for other composite conductive inks.

Data availability statement

The data cannot be made publicly available upon publication because no suitable repository exists for hosting data in this field of study. The data that support the findings of this study are available upon reasonable request from the authors. Data will be available from 2 May 2024.

Acknowledgments

The authors gratefully acknowledge funding support from the National Science Foundation (NSF CMMI-MOMS: 2026936) and by Nextflex (6.6) AWD-003273. The authors are grateful to DuPont colleagues (Jeff Meth, Lynne Dellis and Augustus Jones) for providing samples. This material is based on research sponsored, in part, by Air Force Research Laboratory under agreement number FA8650-20-2-5506, as conducted through the flexible hybrid electronics manufacturing innovation institute, NextFlex. The U.S. Government is authorized to reproduce and distribute reprints for Governmental purposes notwithstanding any copyright notation thereon. The views and conclusions contained herein are those of the authors and should not be interpreted as necessarily representing the official policies or endorsements, either expressed or implied, of Air Force Research Laboratory or the U.S. Government.

Conflict of interest

The authors declare no competing financial interest

ORCID iDs

Olivier Pierron https://orcid.org/0000-0003-0787-7457
Antonia Antoniou https://orcid.org/0000-0002-5270-5438

References

[1] Gao W *et al* 2016 Fully integrated wearable sensor arrays for multiplexed in situ perspiration analysis *Nature* **529** 509–14
[2] Imani S, Bandodkar A J, Mohan A M V, Kumar R, Yu S, Wang J and Mercier P P 2016 A wearable chemical–electrophysiological hybrid biosensing system for real-time health and fitness monitoring *Nat. Commun.* **7** 1–7
[3] Lee H *et al* 2016 A graphene-based electrochemical device with thermoresponsive microneedles for diabetes monitoring and therapy *Nat. Nanotechnol.* **11** 566–72
[4] Stewart B G, Cahn G, Samet D, Misner M J, Burns A, Weerawarne D L, Poliks M D, Lapinski C, Dugan S and Pierron O 2020 Mechanical deformation study of flexible leadset components for electromechanical reliability of wearable electrocardiogram sensors *2020 IEEE 70th Electronic Components and Technology Conf. (ECTC)* (IEEE) pp 532–40
[5] Chow J H, Sitaraman S K, May C and May J 2018 Study of wearables with embedded electronics through experiments and simulations *2018 IEEE 68th Electronic Components and Technology Conf. (ECTC)* (IEEE) pp 814–21
[6] Gebhart D D, Krapf A, Gammer C, Merle B and Cordill M J 2022 Linking through-thickness cracks in metallic thin films to in-situ electrical resistance peak broadening *Scr. Mater.* **212** 114550
[7] Glushko O, Klug A, List-Kratochvil E and Cordill M 2016 Relationship between mechanical damage and electrical degradation in polymer-supported metal films subjected to cyclic loading *Mater. Sci. Eng.* **662** 157–61
[8] Graz I M, Cotton D P and Lacour S P 2009 Extended cyclic uniaxial loading of stretchable gold thin-films on elastomeric substrates *Appl. Phys. Lett.* **94** 071902
[9] Sim G-D, Hwangbo Y, Kim H-H, Lee S-B and Vlassak J J 2012 Fatigue of polymer-supported Ag thin films *Scr. Mater.* **66** 915–8
[10] Sim G-D, Lee Y-S, Lee S-B and Vlassak J J 2013 Effects of stretching and cycling on the fatigue behavior of polymer-supported Ag thin films *Mater. Sci. Eng.* **575** 86–93
[11] Pegan J D, Zhang J, Chu M, Nguyen T, Park S-J, Paul A, Kim J, Bachman M and Khine M 2016 Skin-mountable stretch sensor for wearable health monitoring *Nanoscale* **8** 17295–303
[12] Krawczyk K K, Groten J, Glushko O, Krivec M, Fruühwirth M, Schulz G, Wolf C, Hartmann D, Moser M and Cordill M J 2021 Self-reducing silver ink on polyurethane elastomers for the manufacture of thin and highly stretchable electrical circuits *Chem. Mater.* **33** 2742–55
[13] Matsuhisa N, Inoue D, Zalar P, Jin H, Matsuba Y, Itoh A, Yokota T, Hashizume D and Someya T 2017 Printable elastic conductors by in situ formation of silver nanoparticles from silver flakes *Nat. Mater.* **16** 834–40
[14] Kim J and Kim W S 2014 Stretching silver: printed metallic nano inks in stretchable conductor applications *IEEE Nanotechnol. Mag.* **8** 6–13
[15] Borghetti M, Serpelloni M, Sardini E and Pandini S 2016 Mechanical behavior of strain sensors based on PEDOT: PSS and silver nanoparticles inks deposited on polymer substrate by inkjet printing *Sens. Actuators* A **243** 71–80
[16] Zhang R, Qi L, Lian H and Luo J 2022 Direct printing of surface-embedded stretchable graphene patterns with strong adhesion on viscous substrates *J. Ind. Eng. Chem.* **109** 530–7
[17] Cahn G, Pierron O and Antoniou A 2021 Electrical performance evolution and fatigue mechanisms of silver-filled polymer ink under uniaxial cyclic stretch *Flex. Print. Electron.* **6** 035008
[18] Koshi T, Nomura K-I and Yoshida M 2021 Measurement and analysis on failure lifetime of serpentine interconnects for e-textiles under cyclic large deformation *Flex. Print. Electron.* **6** 025003
[19] Merilampi S, Laine-Ma T and Ruuskanen P 2009 The characterization of electrically conductive silver ink patterns on flexible substrates *Microelectron. Reliab.* **49** 782–90
[20] Mohammed A and Pecht M 2016 A stretchable and screen-printable conductive ink for stretchable electronics *Appl. Phys. Lett.* **109** 184101
[21] Sliz R, Huttunen O-H, Jansson E, Kemppainen J, Schroderus J, Kurkinen M and Fabritius T 2020 Reliability of R2R-printed, flexible electrodes for e-clothing applications *npj Flex. Electron.* **4** 1–9
[22] Suikkola J, Björninen T, Mosallaei M, Kankkunen T, Iso-Ketola P, Ukkonen L, Vanhala J and Mäntysalo M 2016 Screen-printing fabrication and characterization of stretchable electronics *Sci. Rep.* **6** 1–8
[23] Li Q, Antoniou A and Pierron O N 2022 Understanding resistance increase in composite inks under monotonic and cyclic stretching *Flex. Print. Electron.* **7** 045010
[24] Cordill M J, Kreiml P and Mitterer C 2022 Materials engineering for flexible metallic thin film applications *Materials* **15** 926

[25] Hommel M and Kraft O 2001 Deformation behavior of thin copper films on deformable substrates *Acta Mater.* **49** 3935–47
[26] Kaiser T, Cordill M, Kirchlechner C and Menzel A 2021 Electrical and mechanical behaviour of metal thin films with deformation-induced cracks predicted by computational homogenisation *Int. J. Fract.* **231** 223–42
[27] Kraft O, Hommel M and Arzt E 2000 x-ray diffraction as a tool to study the mechanical behaviour of thin films *Mater. Sci. Eng.* **288** 209–16
[28] Lacour S P, Wagner S, Huang Z and Suo Z 2003 Stretchable gold conductors on elastomeric substrates *Appl. Phys. Lett.* **82** 2404–6
[29] Lambricht N, Pardoen T and Yunus S 2013 Giant stretchability of thin gold films on rough elastomeric substrates *Acta Mater.* **61** 540–7
[30] Niu R M, Liu G, Wang C, Zhang G, Ding X D and Sun J 2007 Thickness dependent critical strain in submicron Cu films adherent to polymer substrate *Appl. Phys. Lett.* **90** 161907
[31] Xiang Y, Li T, Suo Z and Vlassak J J 2005 High ductility of a metal film adherent on a polymer substrate *Appl. Phys. Lett.* **87** 161910
[32] Yu D Y and Spaepen F 2004 The yield strength of thin copper films on Kapton *J. Appl. Phys.* **95** 2991–7
[33] Glushko O and Cordill M 2020 In-operando fatigue behavior of gold metallization lines on polyimide substrate *Scr. Mater.* **186** 48–51
[34] Cahn G, Barrios A, Graham S, Meth J, Antoniou A and Pierron O 2020 The role of strain localization on the electrical behavior of flexible and stretchable screen printed silver inks on polymer substrates *Materialia* **10** 100642
[35] Cahn G, Pierron O and Antoniou A 2021 Trace width effects on electrical performance of screen-printed silver inks on elastomeric substrates under uniaxial stretch *J. Appl. Phys.* **130** 115304
[36] Li Q, Chung E, Antoniou A and Pierron O 2023 Modeling resistance increase in a composite ink under cyclic loading *Flex. Print. Electron.* **8** 015014